ELSEVIER

www.elsevier.nl/locate/jorganchem

Journal of Organometallic Chemistry 591 (1999) 36–44

Journal of Organometallic Chemistry

Imido complexes of manganese

Andreas A. Danopoulos [a,*], Jennifer C. Green [b], Michael B. Hursthouse [a]

[a] *Department of Chemistry, University of Southampton, Highfield, Southampton SO17 1BJ, UK*
[b] *Inorganic Chemistry Laboratory, University of Oxford, South Parks Road, Oxford OX1 3QR, UK*

Received 17 June 1999; accepted 22 July 1999

Abstract

The developments in the chemistry of manganese by the use of the imido group (RN^{2-}) are reviewed with emphasis on our own work in the area. The increased kinetic stability of the '$Mn(N^tBu)_3$' fragment enabled the isolation and study of a good number and variety of derivatives in oxidation states V–VII, bearing, amongst others, Mn–C, Mn–N, Mn–S and Mn–O bonds.

Keywords: Manganese; Imido; Alkyl; Amide; Thiolate

1. Introduction

Following the discovery of the first imido complex $OsO_3(N^tBu)$ by Clifford and Kobayashi [1], this area of chemistry has witnessed a tremendous growth, especially in the last decade. The two main directions of research, i.e. (i) the use of the imido ligand as a stabilising or ancillary 'spectator' in organometallic chemistry and catalysis; and (ii) the study of selective transformations involving the imido ligand and a variety of substrates, were greatly facilitated by the refinement of our understanding of the metal–nitrogen multiple bonding. Today, imido complexes are known for the majority of the transition metals, although, those with first row and late transition metals have been more difficult to synthesise but show fascinating reactivity.

Recent developments have been described in a monograph [2] and a review [3]. Part of our contribution to the imido chemistry is related to the discovery of a new family of high oxidation state manganese compounds. A substantial part of this research was developed after the appearance of Wigley's review [3] and therefore a full account of it is now timely. Recent work in the same area by other researchers will also be mentioned.

2. Monomeric d^0 Mn(VII) imido complexes

The history of MnO_4^{n-} ($n = 1, 2$) is long and their chemistry rather well established [4]. Mn_2O_7 and the oxohalides MnO_3X (X = F, Cl) have also been known for a while [4,5], but have been prepared in pure form only relatively recently [5c], mainly because of the difficulties associated with their handling and their thermodynamic instability. All the aforementioned oxo-compounds are powerful and rather unselective oxidants, especially towards organic substrates. These reasons, in combination with the high degree of aggregation and, consequently, inertness of oxo-manganates in intermediate oxidation states (III–V) hampered attempts to synthesise imido analogues of the known oxo complexes. Following well-established synthetic methods [1,2], e.g. treating oxo-compounds with amines, silylamines, isocyanates and phosphinimines, results in uncontrolled oxidations and intractable mixtures. However, the existence of the transient manganese imido intermediates was strongly implicated in the work by Groves and Takahashi [6] who detected the paramagnetic TMPMn(=NCOCF$_3$)(OCOCF$_3$) (TMP = 5, 10, 15, 20-tetramesitylporphyrinato-) after reacting TMP-Mn(N) with $(CF_3CO)_2O$. Later, Mahy et al. [7] postulated manganese imido intermediates in the aziridination of alkenes by tosylimino–iodobenzene (PhI = NTs, Ts = tosyl) catalysed by Mn(TTP)Cl (TTP = tetraphenylporphyrinato). This transformation has been further investigated recently [8].

* Corresponding author. Fax: +44-1703-593-781.
E-mail address: ad1@soton.ac.uk (A.A. Danopoulos)

0022-328X/99/$ - see front matter
PII: S0022-328X(99)00448-9

The first stable isolable manganese imido complex $Mn(N^tBu)_3Cl$ [9,10] was prepared by reaction of acetonitrile solutions of $MnCl_3(NCMe)_3$ [11] with $^tBuNHSiMe_3$. From the green solutions obtained, the imido complex was isolated in ca. 20% yields as a green crystalline, moderately air-stable solid. This unusual transformation is very complex and difficult to study by any spectroscopic methods due to the inhomogeneity and the paramagnetism of the reaction mixture. The only other product isolated from the same reaction mixture was $[MnCl_4][H_3N^tBu]_2$. A sequential oxidation of amido intermediates, $Cl_nMn(NH^tBu)_{3-n}$ $n=1-3$, followed by chlorination of '$Mn(N^tBu)_3$' by the excess of strongly oxidising $MnCl_3$, was proposed [10] as a plausible mechanism accounting for the isolated products and yields. It is interesting to notice at this point that this reaction fails with anilines.

$Mn(N^tBu)_3Cl$ provided a convenient entry to other monomeric Mn(VII) derivatives obtained by simple substitution of the chloride with other anionic groups using thallium or silver salts as transfer reagents [10] as shown in Scheme 1.

Physical data for some of the derivatives obtained are given in Table 1.

Figs. 1 and 2 show the structures of the chloride and pentafluorophenoxide as typical examples, whilst the main structural parameters are summarised in Table 2.

These data show a fairly uniform geometry, with angles around the Mn atom close to tetrahedral, in spite of the differing electronic and steric nature of the

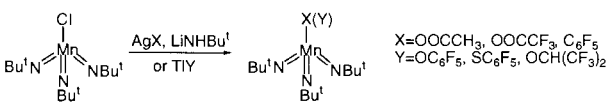

Scheme 1.

Table 1
Monomeric d^0 Mn(VII) derivatives

Compound	Colour	Comments
1 $Mn(N^tBu)_3Cl$	Green	M.p. 94–95°C, NMR, MS, X-ray
2 $Mn(N^tBu)_3Br$	Green	M.p. 105–107°C, NMR, MS
3 $Mn(N^tBu)_3(\eta^1{-}OOCCH_3)$	Green	M.p. 49–59°C NMR, MS, X-ray
4 $Mn(N^tBu)_3(\eta^1{-}OOCCF_3)$	Green	M.p. 95–97°C, NMR, MS
5 $Mn(N^tBu)_3(OC_6F_5)$	Green	M.p. 95–97°C, NMR, MS, X-ray
6 $Mn(N^tBu)_3(SC_6F_5)$	Green	M.p. 121–122°C, NMR, MS, X-ray
7 $Mn(N^tBu)_3(C_6F_5)$	Green	Oil, $t_{1/2}$ ca. 3 h at r.t., NMR, MS
8 $Mn(N^tBu)_3(NH^tBu)$	Green	Oil, $t_{1/2}$ ca. 1 h at r.t., NMR, MS
9 $Mn(N^tBu)_3[OCH(CF_3)_2]$	Green	Oil, NMR, MS

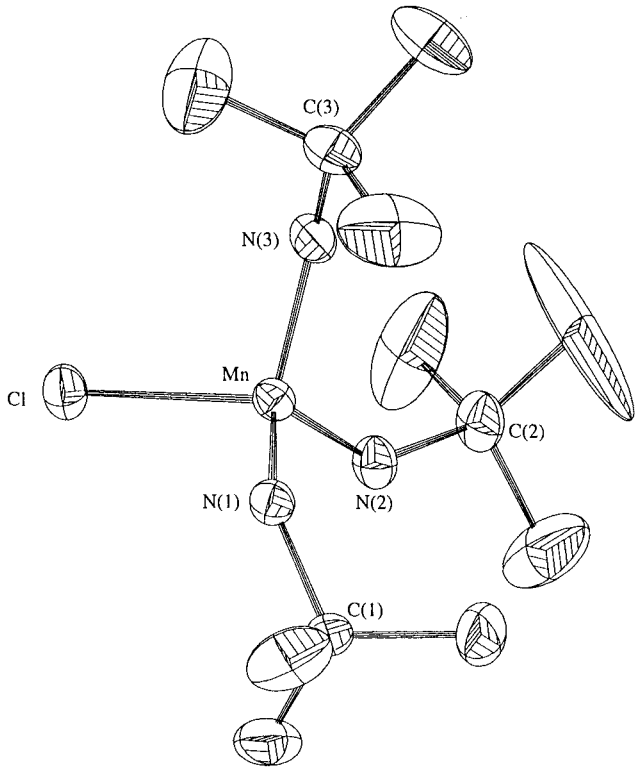

Fig. 1. The structure of the tris-imido chloride.

X ligands. Of particular note is the consistency of the Mn-imido geometry, where the Mn–N distances lie within the short range 1.644–1.673 Å, with an average of 1.656 Å, and the Mn–N–C angles are all close to an intermediate value of 140°. These geometrical features have been explored via density functional theory (DFT) calculations (see below).

The high thermal stability of the imido analogues is striking when compared with their known oxo counterparts, a fact ascribed to kinetic stabilisation by the imido groups. By taking advantage of this, $Mn(N^tBu)_3(C_6F_5)$ (**7**) was prepared bearing a Mn-(VII)–carbon bond; **7** was sufficiently stable to be isolated as oil at room temperature (r.t.) and identified spectroscopically [10].

An insight into possible decomposition pathways operating with these high oxidation state compounds was gained by studying the product distribution from the decomposition of $(^tBuN)_3MnOC(H)(CF_3)_2$ (**10**). This occurred as shown schematically in Scheme 2 by transfer of the β-hydrogen to the basic nitrogen of the imido group.

The formation of the manganate nitride dianion **10**, which has been structurally characterised (see Fig. 3) has been rationalised by the reaction sequence shown in Scheme 3 [12].

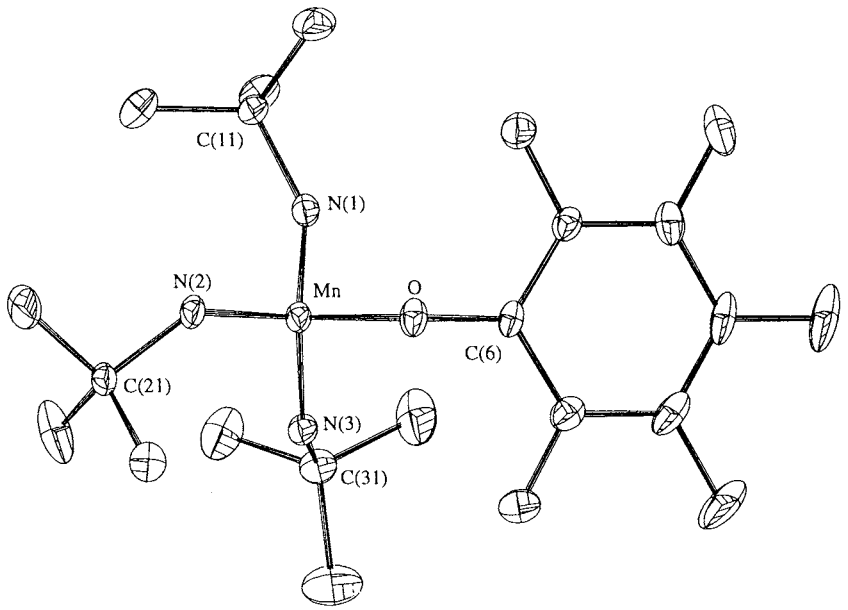

Fig. 2. The structure of the tris-imido pentafluorophenoxide.

Table 2
Structural data for mononuclear $Mn(N^tBu)_3X$ derivatives [a]

X	Mn–X (Å)	Mn–N (Å)	X–Mn–N (°)	N–Mn–N (°)	Mn–N–C (°)
Cl	2.222(3)	1.656(3)	107.3(2)	111.6(2)	140.3(3)
η^1-O_2CMe	1.91(3)	1.660(5)	106.8(7)	112.0(3)	142.3(3)
OC_6F_5	1.896(2)	1.657(1)	107.7(1)	111.2(1)	140.8(2)
SC_6F_5	2.289(1)	1.651(2)	105.8(1)	112.9(1)	142.6(6)

[a] Values represent averages for each compound.

In the structure, the Mn-imido bonding parameters reflect decreased π-bonding for the three imido ligands, with increased Mn–N bond lengths [average 1.763(3) Å] and reduced Mn–N–C angles of ca. 130°.

3. Electronic structure of $Mn(N^tBu)_3Cl$

DFT calculations [13] have been used to model the structure and photoelectron spectrum of $Mn(N^tBu)_3Cl$. The calculations were carried out on $Mn(NMe)_3Cl$. Good agreement was found between the experimental and calculated distances and angles (Table 3) in contrast with a previous report [14].

The one-electron energies are shown diagramatically in Fig. 4. The metal character of the orbitals is given in Table 4. The energy grouping of the ligand π orbitals bears a close resemblance to that expected for a d^0 tetrahedral structure and bears witness to the close resemblance of this species to the permanganate ion. Though the C_3 symmetry of the molecule is such that all ligand combinations can in principle mix with metal orbitals, in effect the non-bonding t_1 ancestry of the top three occupied orbitals means that they are principally located on the ligands. The main mixing with the metal occurs in the 1e orbitals. The 1a orbital is Mn–Cl σ bonding.

The PE spectrum is shown in Fig. 5. Ionisation energies (IEs) were calculated for $Mn(NMe)_3Cl$ by taking the difference between the appropriate ion state energy and that of the molecule. All calculated IEs were somewhat higher than those found experimentally. This is expected as a methyl substituent to be less donating than a *t*-butyl one. However, the grouping of the calculated IE is in excellent agreement with the spectrum and helps confirm the one-electron model revealed by the calculation. The picture is reinforced by the He-

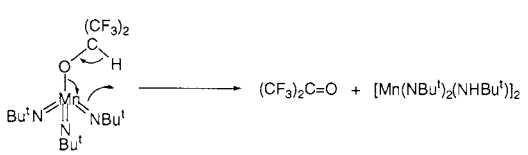

Scheme 2.

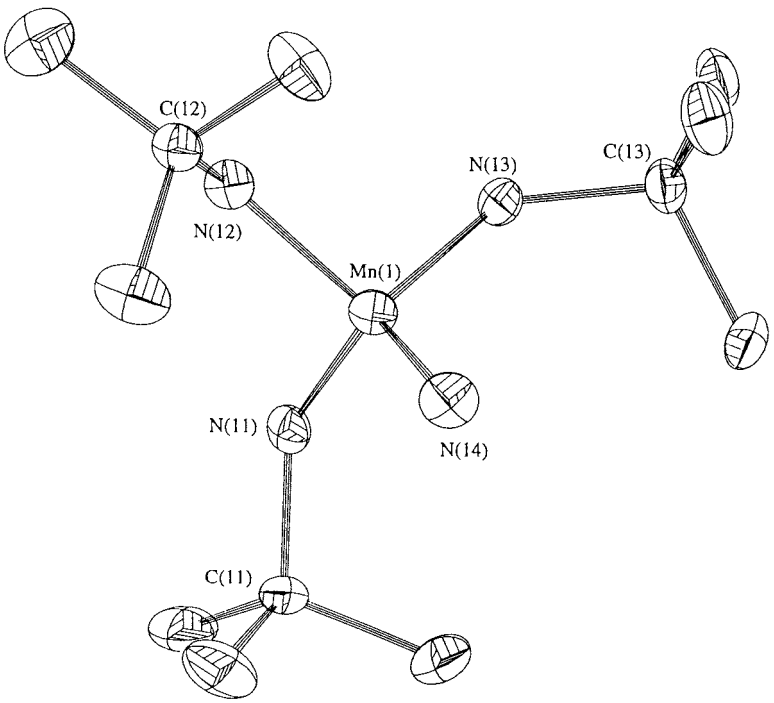

Fig. 3. The structure of the nitride dianion in $[Li(OEt_2)_2]_2(^tBuN)_3MnN]$ (**10**).

I and He II intensity patterns, which indicate that band C, assigned to the 1e ionisation, has the maximum amount of Mn *d* character.

The origin of the bending of the imido ligand was investigated by optimising the structure of Mn-$(NMe)_3Cl$ with C_{3v} symmetry and with the Mn–N–C bond angles fixed at 180°. The final structure was found to be 55 kJ mol^{-1} higher in energy than the C_3 structure. The one-electron energies are given in Fig. 5. The biggest shift in energy was found in the HOMO which was raised in energy by 1.2 eV on straightening the imido groups. This orbital is imido-localised in both geometries; schematic representations are also shown in Fig. 4. As the orbital is not bonding in either geometry, we attribute its energy change to its N–N antibonding character, which is enhanced when the imido groups are linear. Bending decreases the interaction between the electron pairs on the N atoms. The effect is less in the 3e orbitals as they also have Cl pπ character so the effect of the N pπ repulsion is attenuated in this orbital set.

A comparison of the bonding of $Mn(N^tBu)_3Cl$ with $Re(N^tBu)_3Cl$ will appear in due course.

4. Monomeric d^1 Mn(VI) imido complexes

Reaction of the complex $Mn(N^tBu)_3Cl$ with five equivalents of $LiNH^tBu$ in dme (dme = 1,2-dimethoxyethane) or tmed (tmed = *N*,*N*,*N*′,*N*′-tetramethylethylenediamine) gave good yields of the purple crystalline $[(^tBuN)_4Mn]^{2-}$ as Li(dme) **11a** or Li(tmed) **11b** adducts, both of which were structurally characterised; Fig. 6 shows the structure of **11a**. This paramagnetic anion is the imido analogue of the well-known MnO_4^{2-}. Its reactivity with electrophilic reagents is shown in Scheme 4 [10].

5. Di- and tri-nuclear d^1 Mn(VI) and d^2 Mn(V) imido complexes

The dinuclear core $[Mn_2(\mu\text{-}N^tBu)_2]^{n+}$ ($n = 6, 7, 8$) is a common structural motif encountered in manganese imido complexes, in which the metals have oxidation states VI or V. The chemical transformations within this group of compounds are given in Scheme 5 [15].

The observed diamagnetism of the dimers **12** and **14** is ascribed to metal–metal interaction. High-accuracy structural data for these compounds are not available due to persistent twinning of the crystals obtained. However, the intermetallic distance in the paramagnetic

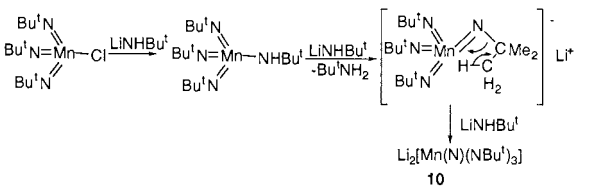

Scheme 3.

Table 3
Comparison of calculated and experimental geometries of $Mn(NR)_3Cl$

	Mn–N (Å)	Mn–Cl (Å)	N–C (Å)	Mn–N–C (°)	Cl–Mn–N (°)	N–Mn–N (°)
$Mn(NMe)_3Cl$ (calculated)	1.63	2.16	1.40	133	109	110
$Mn(N^tBu)_3Cl$ (experimental)	1.66	2.22	1.46	140	108	111

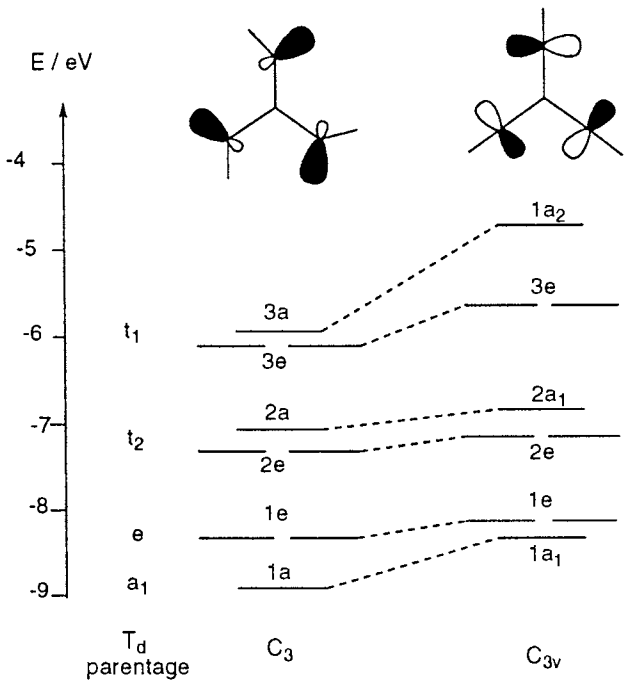

Fig. 4. Orbital energy diagram and schematic representation of the HOMOs of $(MeN)_3MnCl$ in C_3 and C_{3v}. The symmetry of the related T_d orbitals is given on the left.

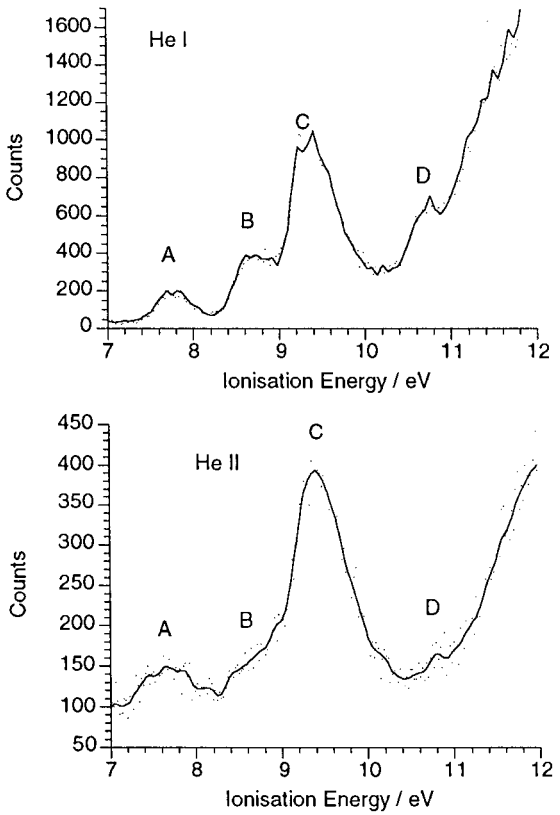

Fig. 5. He I and He II spectra of $(^tBuN)_3MnCl$.

Table 4
Experimental IEs (eV) for $Mn(N^tBu)_3Cl$ [a]

MO	IE (experimental)	IE (calculated)	ε_i	% *d*
3a	7.75 A	8.37	−5.95	<1
3e		8.60	−6.08	7
2a	8.63 B	9.52	−7.05	10
2e		9.71	−7.31	15
1e	9.38 C	10.78	−8.28	47
1a	10.71 D	11.80	−8.80	27

[a] Calculated IEs and orbital energies (ε_i) for $Mn(NMe)_3Cl$ and *d* character of the associated MO.

dimer **13** (Fig. 7) at 2.587(2) Å is consistent with strong interaction between the metal centres, as is the average Mn–N–Mn angle of 90.0(2)°.

Heterometallic complexes have also been prepared and structurally characterised. For example, interaction of the Mn(VI)–Mn(VI) homoleptic imido complex **12** with Me_2Zn gave the linear paramagnetic trimetallic complex **16** shown in Fig. 8 with two distinct manganese centres.

Alkylation of $Mn(N^tBu)_3Cl$ using an excess of β-elimination stabilised zinc alkyls gave rise to the first thermally stable, diamagnetic Mn(V) alkyls, $[(^tBuN)(R)Mn(\mu\text{-}N^tBu)]_2$ (R = Me, Et, CH_2^tBu, CH_2Ph, CH_2SiMe_3, CH_2Me_2Ph) [12]. The neopentyl, R = CH_2^tBu, and benzyl, R = CH_2Ph, have been structurally characterised and the structure of the former is shown in Fig. 9. Both were found to adopt the *Z* (or *cis*) arrangement. This is different to the situation found in the $[TcMe_2(NAr')(\mu\text{-}NAr')]_2$ [16], where the observed arrangement is *E*(*trans*). The Mn–C distances 2.041 and 2.062 Å are shorter than those found in the Mn(IV) species $MnMe_4(dmpe)$ [17] [dmpe = 1,2-bis-(dimethylphosphino)ethane], $[MnMe_6]^{2-}$ [18] and the Mn(II) alkyls [19]. In toluene solution, isomerisation to a mixture of *Z* and *E* isomers is detected by ^{1}H-NMR spectroscopy after 2 weeks (Scheme 6). This presumably occurs by the opening of the Mn_2N_2 ring [15].

A simple explanation for the thermal stability of **17** is that the metal atoms are coordinatively saturated and

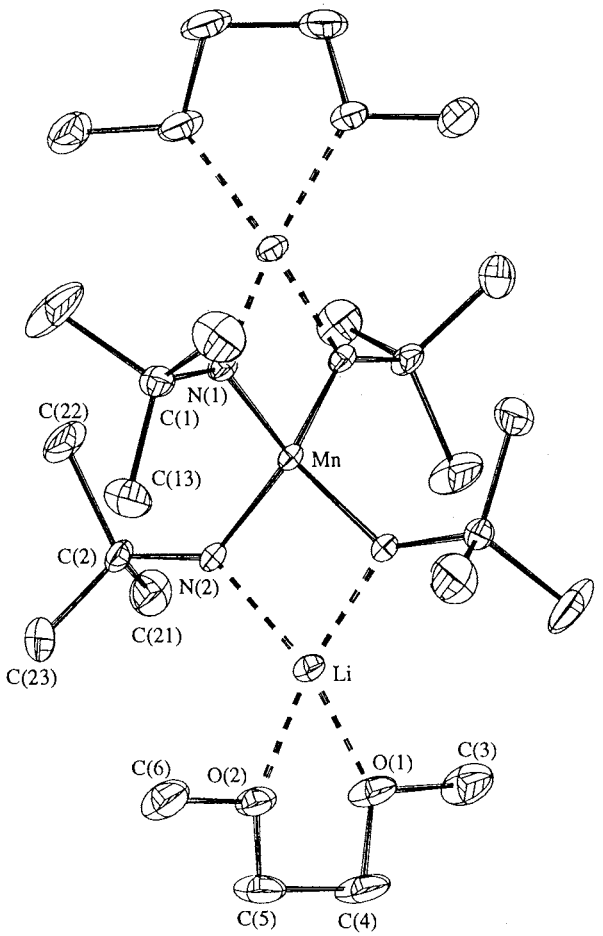

Fig. 6. The structure of the complex $[Li(dme)]_2[Mn(N^tBu)_4]$ (**11a**).

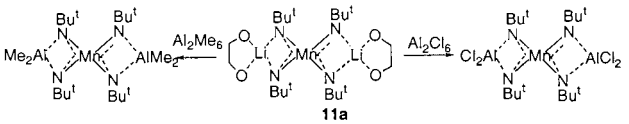

Scheme 4.

pathways for decomposition involving β-H transfer are not available.

Trinuclear mixed-valence diamagnetic manganese cations are obtained by 'oxidative de-imidation' of $[(^tBuN)_2Mn(\mu\text{-}N^tBu)]_2$ (**12**) with I_2 [15] (Scheme 5). The structure of **15** is shown in Fig. 10. The imido bridges are strongly unsymmetrical with the Mn–N distances to the outer Mn atoms 1.87 and to the inner 1.77 Å. This asymmetry has been rationalised in terms of competition for $N \rightarrow Mn$ π-bonding involving terminal and bridging imido groups [15].

Finally, an interesting reaction has been observed by attempted oxidation of $[(^tBuN)_2Mn(\mu\text{-}N^tBu)]_2$ (**12**) with Ag^+ salts. In CH_2Cl_2 solutions an imido nitrogen centred radical is formed, detected by (i) the selective paramagnetic broadening of the terminal imido peak in

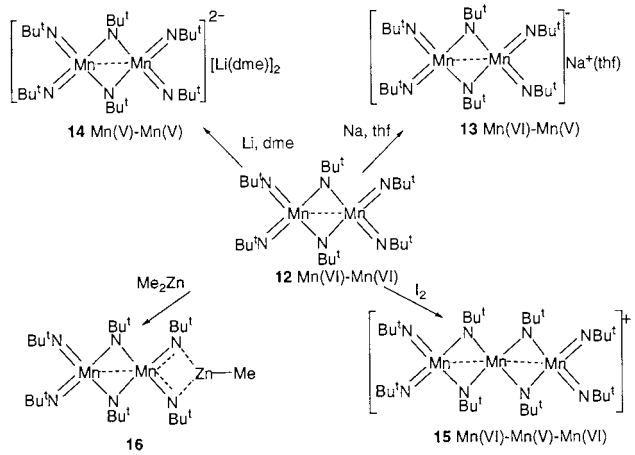

Scheme 5.

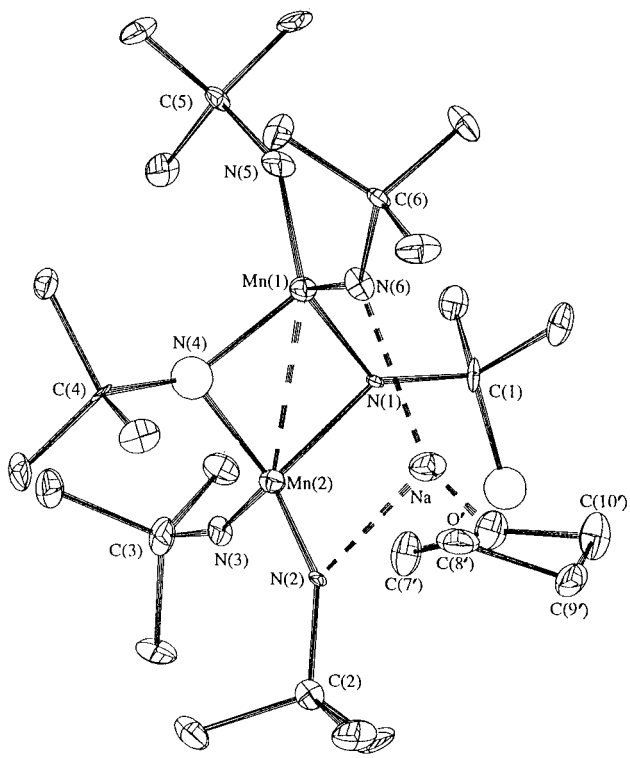

Fig. 7. The structure of the complex $\{Na(thf)][\{(^tBuN)_2Mn(\mu\text{-}N^tBu)\}_2]$ (**13**).

the ^{1}H-NMR spectrum and (ii) the appearance of a triplet with $g = 2.00$ and $\alpha_N = 15G$ in the X-band EPR spectrum. In thf solutions this free radical abstracts $H^\bullet$ from the solvent giving rise to **19** (Scheme 7), or reacts with O_2 to produce the mixed oxo-imido-linear trinuclear cation **18**, which has been structurally characterised [13] (Fig. 11).

The formation of cation radical intermediates has been suggested by Mahy et al. in the aziridination of olefins by $[(TPP)Mn(=NTs)]^+$ catalysts [7].

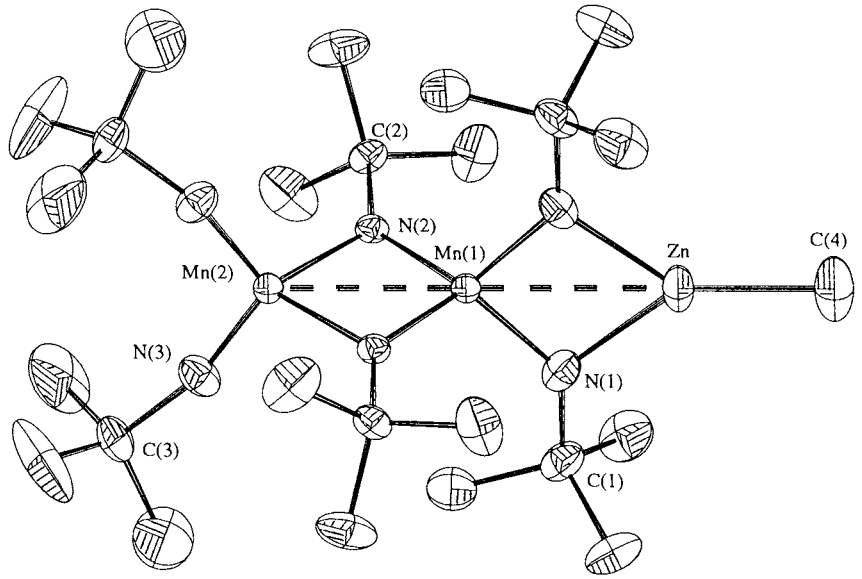

Fig. 8. The structure of the zinc complex **16**.

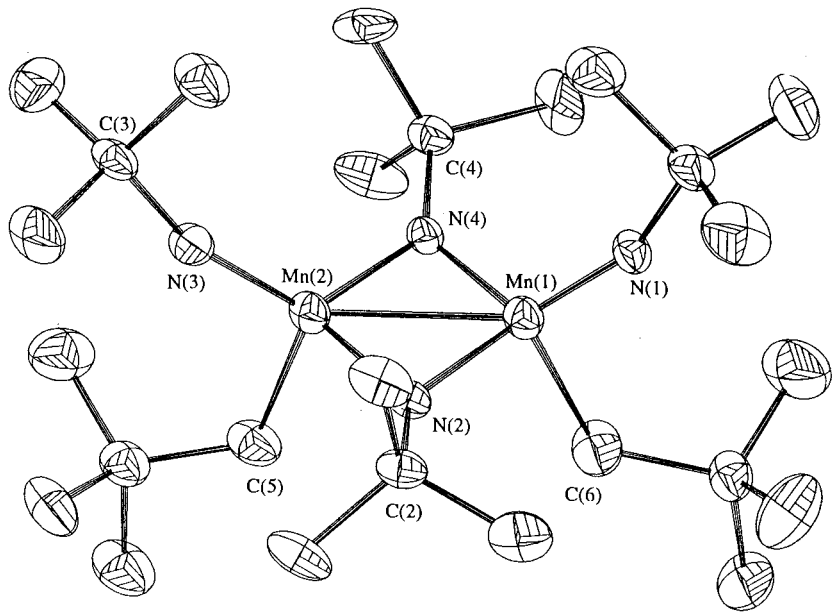

Fig. 9. The structure of $[(^{t}BuN)_2(CH_2Me_3)Mn(\mu\text{-}N^{t}Bu)]_2$.

As previously mentioned, the $[Mn_2(N^{t}Bu)_2]$ dimer unit is widespread amongst these multinuclear species and its character and environment vary considerably. However, detailed analysis of the Mn_2N_2 geometry shows some interesting systematics. Irrespective of the bond length variations which range from 1.72 to 1.88 Å, the average Mn–N(bridge) distances in a given unit lies in the narrow range of 1.81 ± 0.01 Å. As a result, whilst the shape of the Mn_2N_2 ring varies according to the degree of Mn···Mn bonding, and the symmetry or asymmetry of the Mn environments, there is almost perfect correlation between the Mn···Mn distance and

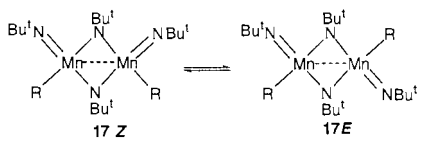

Scheme 6.

the Mn–N–Mn angle. At the same time, it is pertinent to note that in the multinuclear species, where all truly terminal imido functions are linear (i.e. those which are not involved in interactions with Li or Na cations), the Mn–N distances are also very similar, at 1.63 ± 0.02 Å.

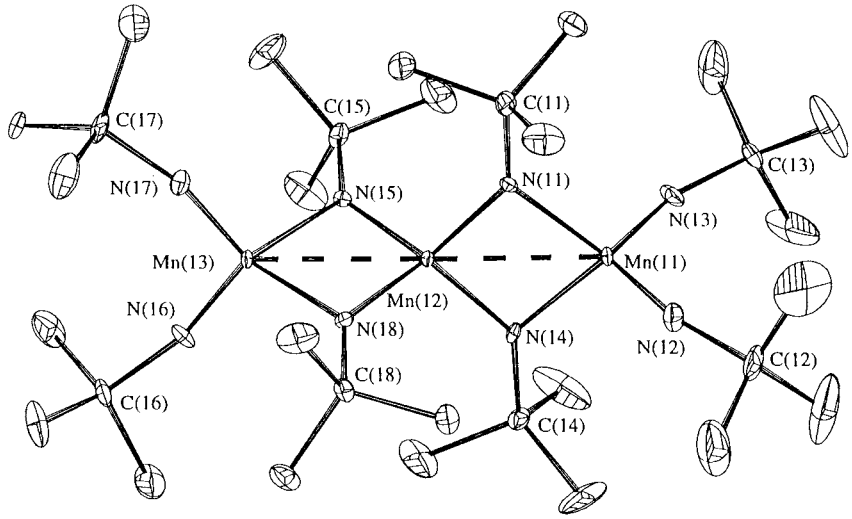

Fig. 10. The structure of the trimeric cation in complex **15**.

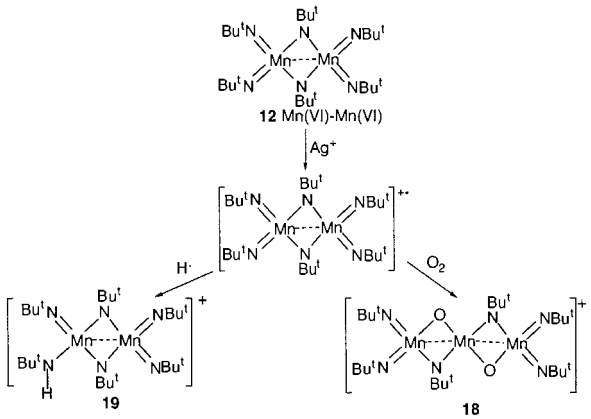

Scheme 7.

These data strongly indicate that charge or oxidation state formalisms are not important in determining the electron distribution around this core unit.

6. d^5 Mn(II) arylimido complexes

Grigsby and Power have reported [20] that interaction of $MnBr_2$ with the imide transfer reagent $\{Mg(NPh)(thf)\}_6$, thf = tetrahydrofuran, gave the polynuclear manganese (II) imido compounds $[\{Mn_6(\mu^3\text{-}NPh)_4Br_3(thf)_4\}\{Mg_2(\mu\text{-}NHPh)\text{-}(\mu\text{-}Br)Br_2(thf)_4\}]$and $Mn_6(\mu^3\text{-}NPh)_4Br_4(thf)_6$, which have been characterised

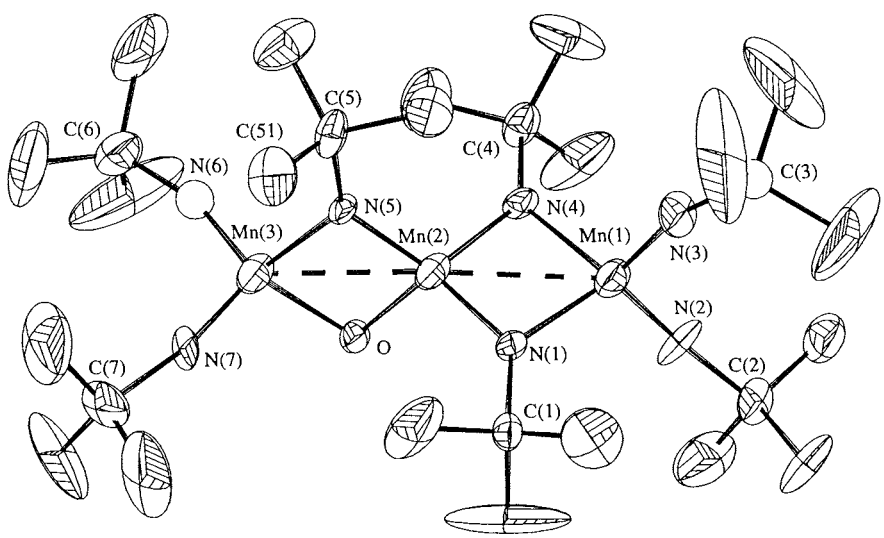

Fig. 11. The structure of the cationic oxo-bridged trimer **18**.

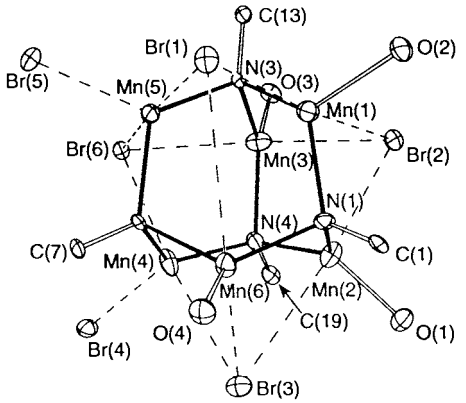

Fig. 12. The structure of $[Mn_6(\mu_3\text{-}NPh)_4Br_3(thf)_4]^+$. Only *ipso* carbons of the phenyl rings and oxygen atoms of the thf molecules are shown.

crystallographically and exhibit adamantane-like Mn_6N_4 structures (Fig. 12).

Acknowledgements

The authors thank Steven J. Dixon for carrying out the PE measurements and Joanne Wallace for the DFT calculations. A.A.D. is indebted to the Wilkinson Trust Fund and the EPSRC for financial support during this work.

References

[1] A.F. Clifford, C.S. Kobayashi, Abstracts, 130th National Meeting of the ACS, Atlantic City, NJ, 1956, p. 50R.
[2] W.A. Nugent, J.M. Mayer, Metal–Ligand Multiple Bonds, Wiley, New York, 1988.
[3] D.E. Wigley, Prog. Inorg. Chem. 42 (1994) 239.
[4] J.W. Mellor, A Comprehensive Treatise on Inorganic and Theoretical Chemistry, vol. 12, Longman Green, London, 1932.
[5] (a) A. Simon, Z. Anorg. Allg. Chem. 558 (1988) 7. (b) A. Engelbrecht, A. v Grosse, J. Am. Chem. Soc. 76 (1954) 2042. (c) A.K. Brisdon, J.H. Holloway, E.G. Hope, P.J. Townson, W. Levason, J.S. Ogden, J. Chem. Soc. Dalton Trans. (1991) 3127.
[6] J.T. Groves, T. Takahashi, J. Am. Chem. Soc. 105 (1983) 2073.
[7] J.P. Mahy, G. Bedi, P. Battioni, D. Mansuy, Tetrahedron Lett. 29 (1988) 1927.
[8] J. du Bois, C.S. Tomooka, J. Hong, E.M. Carreira, Acc. Chem. Res. 30 (1997) 364, and references cited therein.
[9] A.A. Danopoulos, G. Wilkinson, T.K.N. Sweet, M.B. Hursthouse, J. Chem. Soc. Chem. Commun. (1993) 495.
[10] A.A. Danopoulos, G. Wilkinson, T.K.N. Sweet, M.B. Hursthouse, J. Chem. Soc. Dalton Trans. (1994) 1037.
[11] S.P. Perlepes, A.G. Blackman, J.C. Huffman, G. Christou, Inorg. Chem. 30 (1991) 1665.
[12] A.A. Danopoulos, G. Wilkinson, T.K.N. Sweet, M.B. Hursthouse, J. Chem. Soc. Dalton Trans. (1995) 205.
[13] G. te Velde, E.J. Baerends, J. Comput. Phys. 99 (1992) 84.
[14] M.S. Gordon, T.R. Cundari, Coord. Chem. Rev. 147 (1996) 87.
[15] A.A. Danopoulos, G. Wilkinson, T.K.N. Sweet, M.B. Hursthouse, J. Chem. Soc. Dalton Trans. (1995) 937.
[16] A.K. Burrell, O.C. Bryan, Organometallics 12 (1993) 2426.
[17] C.G. Howard, G.S. Girolami, G. Wilkinson, M. Thornton-Pett, M.B. Hursthouse, J. Chem. Soc. Chem. Commun. (1983) 1163.
[18] R.J. Morris, G.S. Girolami, Organometallics 10 (1991) 792.
[19] P.R. Raithby, PhD Thesis, University of London, 1976.
[20] W.J. Grigsby, P.P. Power, J. Chem. Soc. Dalton Trans. (1996) 4613.